Proc. Natl. Acad. Sci. USA
Vol. 93, pp. 10769–10774, October 1996
Biophysics

Direct evidence for modified solvent structure within the hydration shell of a hydrophobic amino acid

ALEXANDER PERTSEMLIDIS*, ANAND M. SAXENA†, ALAN K. SOPER‡, TERESA HEAD-GORDON§, AND ROBERT M. GLAESER§¶‖

*Graduate Group in Biophysics and ¶Department of Molecular and Cell Biology, University of California, Berkeley, CA 94720; †Biology Department, Brookhaven National Laboratory, Upton, NY 11973; ‡ISIS Facility, Rutherford Appleton Laboratory, Chilton, Didcot, Oxon OX11 0QX, United Kingdom; and §Life Sciences Division, Lawrence Berkeley National Laboratory, Berkeley, CA 94720

Communicated by Frank H. Stillinger, Bell Laboratories, Murray Hill, NJ, June 12, 1996 (received for review March 21, 1996)

ABSTRACT **Neutron scattering experiments are used to determine scattering profiles for aqueous solutions of hydrophobic and hydrophilic amino acid analogs. Solutions of hydrophobic solutes show a shift in the main diffraction peak to smaller angle as compared with pure water, whereas solutions of hydrophilic solutes do not. The same difference for solutions of hydrophobic and hydrophilic side chains is also predicted by molecular dynamics simulations. The neutron scattering curves of aqueous solutions of hydrophobic amino acids at room temperature are qualitatively similar to differences between the liquid molecular structure functions measured for ambient and supercooled water. The nonpolar solute-induced expansion of water structure reported here is also complementary to recent neutron experiments where compression of aqueous solvent structure has been observed at high salt concentration.**

Interest in the structural organization of the solvent within the hydration shell of amino acid side chains arises partly from questions related to the thermodynamic and structural explanations of the hydrophobic interaction between nonpolar side chains. Much thermodynamic evidence is conventionally interpreted as indicating a differently organized structure of the water that is in contact with a nonpolar solute as compared with the pure liquid (1, 2). As one example, there is a significant increase in heat capacity when proteins are unfolded or when hydrophobic compounds are dissolved in water, and this change in heat capacity is a linear function of the area of the hydrophobic surfaces (3, 4). The large and positive heat capacity change is normally attributed to the extra heat needed to "melt" the ordered water structure near hydrophobic groups exposed to water. As a second example, departures from ideality in the observed freezing-point depression of aqueous solutions of amino acids support the picture that there are significant structural changes within the hydration shell of amino acid side chains (5). Once again, the observed effect (in this case, nonideality) is a linear function of the exposed surface area.

The relationship between water structure and the hydrophobic effect has also been the subject of a number of theoretical studies (6, 7) and computer simulations (8–13) on a number of model side chain solutes. Structural analyses of the simulation data indicate that water retains its hydrogen-bonded network by "straddling" the surface of the nonpolar group with three of its four tetrahedral hydrogen bonds, with the fourth bond pointing away from the hydrophobic surface. Neutron scattering experiments have provided confirmation of this view, where water molecules are observed to lie roughly tangential to the surface of the nonpolar solute (14, 15). Further experimental evidence for a hydrogen-bonded hydration shell around hydrophobic groups is found in the x-ray crystal structures of clathrate compounds (16). In these solid, crystalline hydrates, water molecules are organized completely into hydrogen-bonded polygons that enclose the nonpolar guest, with pentagons occurring much more frequently than in bulk water, outnumbering hexagons by about eight to one for small solutes. These clathrate structures are normally invoked as representing a model of what the structure of liquid water might be in the immediate vicinity of a nonpolar solute molecule (8–13); recent molecular dynamics simulations analyzed in terms of water hydrogen-bonded polygons support the view that clathrate analogies are useful for describing liquid water structure near hydrophobic solutes (17).

If the water of hydration was to adopt a sufficiently large modification in structure relative to that of bulk water, it should result in a measurable difference of the wide angle scattering pattern in the region of the so-called "water ring," the main diffraction peak at $Q \approx 2.0$ Å^{-1} for water at room temperature. We report in this paper our observation of a shift in the main diffraction peak by ≈ 0.05 Å^{-1} for aqueous solutions of molecules with hydrophobic, but not hydrophilic, side chains, using both neutron scattering experiments and molecular dynamics simulations.

The observed change between aqueous solutions of hydrophobic groups and bulk water at room temperature is analogous to changes that have been observed between ambient temperature water and supercooled water, a shift in the main diffraction peak to smaller Q (18–20). Stillinger (2) and Speedy (21, 22) have noted the possible geometric connection between water near hydrophobic groups and that of supercooled water. It is proposed that supercooled water and hydration water share a common structural feature, namely polyhedral cages of hydrogen bonds that, because they are unstrained and unbent, are more expanded than the continuous random network within which they are rather easily embedded (2). Recently reported neutron diffraction experiments on highly concentrated salt solutions exhibit the opposite effect: a shift to larger Q in the $g_{HH}(r)$ partial correlation function (23). In this case, the strong electric field of the ion overwhelms the usual "quality" of hydrogen-bonding interactions between water molecules in the hydration shell or with the interfacing bulk, so that the shift to larger Q can be interpreted as evidence for particularly strained hydrogen-bonds and, therefore, compressed water structure.

EXPERIMENTAL METHODS AND DESIGN

Neutron Scattering Experiments. Neutron scattering intensities were measured (24) on beamline H3B at the High Flux Beam Reactor (HFBR) at Brookhaven National Laboratory

The publication costs of this article were defrayed in part by page charge payment. This article must therefore be hereby marked "*advertisement*" in accordance with 18 U.S.C. §1734 solely to indicate this fact.

Abbreviations: HFBR, High Flux Beam Reactor; NALA: *N*-acetylleucine amide; NAKA, *N*-acetyllysine amide; NAGA, *N*-acetylglycine amide; NAQA, *N*-acetylglutamine amide.

‖To whom reprint requests should be addressed.

for solutions of *N*-acetylleucine amide (NALA) in D_2O at three different concentrations (0.125, 0.5, and 1.0 M). Similar measurements were also made for 0.5 M isobutanol (model leucine side-chain), 0.43 M *N*-acetylglycine amide (NAGA; a model backbone), and for two hydrophilic solutes, 0.5 M *N*-acetyllysine amide (NAKA) and 0.26 M *N*-acetylglutamine amide (NAQA). All experimental runs reported here were at room temperature.

Two samples were prepared for each solute: (*i*) one consisting of nondeuterated solute dissolved in ^2H_2O, and (*ii*) one, representing the solvent only, in which H_2O was added to ^2H_2O to match the hydrogen-deuterium exchange between the solute (exchangeable hydrogens on nitrogen) and the solvent in the first sample. The purpose of these two measurements is to subtract the scattering measured for pure water from that of the aqueous solution. In addition, an 8% solution of ^2H_2O in H_2O was used as an isotropic scatterer. Approximately 1 ml of each sample was placed into a quartz cuvette with a path length of 5 mm and wall thickness of 2.5 mm; the cuvette was sealed with a Teflon plug. All samples and an empty cuvette were moved into the neutron beam by an automatic sample changer, which repeatedly alternated samples so that any changes in the beam characteristics over time would not disproportionately affect any one sample. Individual frames (i.e., two-dimensional detector images) were summed, and the sum was normalized by the number of counts recorded in the incident beam monitor and by the measured transmission of the sample. The scattering from the empty cuvette was then subtracted from all measurements. Corrections for the flat-plane detector geometry and for variations in sensitivity in different pixels were combined in a single operation by normalizing the image of the measured scattering by that from the isotropic scatterer. Circular integration of the two-dimensional detector images gave the one-dimensional scattering curve, $I(Q)$.

Neutron scattering data were also collected at the SANDALS neutron-scattering spectrometer at the ISIS facility at Rutherford Appleton Laboratory for the 0.5 M solution of NALA and for the corresponding solvent (water) as described above. The sample holder used on the SANDALS spectrometer was made of a null-scattering zirconium-titanium alloy, holding a planar slab of liquid that was 1-mm thick. Data were corrected for background, multiple scattering, absorption, and inelasticity effects, and converted first to the absolute scale of barns per steradian per atom (25). Multiplication by a factor of three gives the differential cross section as the scattering per water molecule, rather than the scattering per atom.

The HFBR data were placed on the same scale as the SANDALS data by a two-parameter fit in which a constant (i.e., isotropic scattering) term was subtracted as an empirical correction for multiple scattering, and the remainder was scaled to the SANDALS curves by a constant. The two parameters were chosen so as to give a least squares best fit of the 0.5 M NALA data from HFBR to the differential cross sections derived from the SANDALS data, and these same parameters were then applied to all of the other samples measured at HFBR.

The scattering measured for pure water was scaled by k, the estimated number of water molecules per unit volume of a given solution divided by the number of water molecules per unit volume of pure water. The scaled intensity for pure water was then subtracted from the scattering intensity for the appropriate solution. The resulting "excess scattering"

$$I_{\text{excess}}(Q) = I_{\text{solution}}(Q) - kI_{\text{pure water}}(Q) \qquad [1]$$

provides a sensitive way to indicate the extent to which the scattering from the aqueous solution differs from the scattering that is produced by pure water.

Molecular Dynamics Simulations. Molecular dynamics simulations of leucine and glutamine *N*-acetyl amino acid methylamide were calculated using the parameter set of AMBER 4.0 (26) with 502 SPC (27) water molecules at 298 K and 1 atm. Our atomic models of the leucine- and glutamine-based solutes are identical to the experimental solutes except for a difference in the C-terminal blocking group, where the simulation uses the traditional methylamide blocking group. An independent simulation of pure water using 512 SPC water molecules was performed to generate the excess scattering curves, $I_{\text{excess}}(Q)$. The SPC water and AMBER solute parameters are well-adapted for simulations at room temperature and pressure.

To generate a scattering intensity curve, $I(Q)$, we first evaluate radial distribution functions, $g_{AB}(r)$, and then use them to generate partial structure factors, $H_{AB}(Q)$, according to the formula,

$$H_{AB}(Q) = 4\pi\rho\int_0^\infty r^2[g_{AB}(r) - 1]\frac{\sin(Qr)}{Qr}\,dr, \qquad [2]$$

where ρ is the number of atoms (of all types) per unit volume. Neutron scattering lengths, b, appropriate to each nucleus are then used to generate the scattering curve from the sum

$$I(Q) = \sum_A\sum_B c_A c_B b_A b_B H_{AB}(Q), \qquad [3]$$

where c_A and c_B are the fractional atomic concentrations for atoms of each type, and the symbols b_A and b_B represent the coherent scattering lengths.

The excess scattering function for the aqueous *N*-acetyl amino acid methylamide solutions is composed of three contributions

$$I_{\text{excess}}(Q) = I_{\text{solute-solute}}(Q) + I_{\text{solute-water}}(Q) + \Delta I_{\text{water-water}}(Q). \qquad [4]$$

We can estimate the contribution $\Delta I_{\text{water-water}}(Q)$ by using only the radial distribution functions $g_{OO}(r)$, $g_{OD}(r)$, and $g_{DD}(r)$ for pure water and for the solution, and taking the difference of the water scattering curves generated from them exactly as in Eq. **1**. The contribution due to correlations between solute molecules and water molecules, $I_{\text{solute-water}}(Q)$, is estimated in a similar way, beginning with the corresponding radial distribution functions $g_{AB}(r)$, where A designates one of the chemically distinguishable atomic species on the solute and B designates either oxygen or deuterium in the solvent.

RESULTS

Fig. 1*A* shows the measured differential scattering cross-section as a function of momentum transfer, $Q = (4\pi/\lambda)\sin(\theta/2)$, for 0.5 M NALA and for pure water, which were collected on the SANDALS neutron-scattering spectrometer. The large offset between the two curves in Fig. 1*A* is due to the additional isotropic scattering that is associated with the solute. The additional scattering due to the presence of the solute is automatically expressed as an excess amount of scattering per water molecule, as a result of the data reduction described above.

The measured excess scattering, Eq. **1**, is shown in Fig. 1*B*. The increased amount of small-angle scattering seen in Fig. 1*B* was expected due to the presence of solute molecules in the solution, and it is likely to contain contributions from both $I_{\text{solute-solute}}(Q)$ and $I_{\text{solute-water}}(Q)$, as written in Eq. **4**. The small peak in the excess scattering appearing on the low Q side of the water ring, which was followed immediately by a dip in the curve, was not anticipated, however. Close examination of the curves in Fig. 1*A* shows that it is possible to detect a slight shift of the water peak to lower Q for the scattering from the solution. As will be shown here, this perturbation in the water

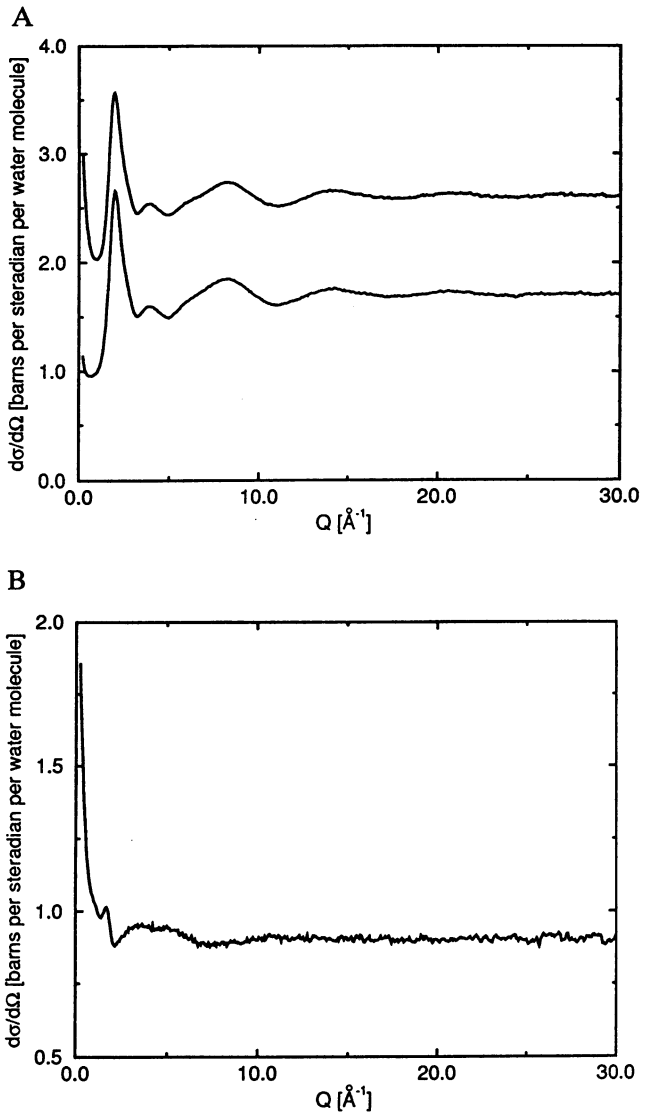

FIG. 1. (*A*) Differential scattering cross sections for a 0.5 M solution of NALA (upper curve) and the corresponding solvent (lower curve) measured at the ISIS facility. The large peak at $Q \approx 2.0$ Å^{-1} is referred to as the (characteristic) water ring, which occurs at an effective Bragg spacing that is similar to that of the first-order diffraction peaks for hexagonal ice. (*B*) Excess scattering intensity for the 0.5 M NALA solution, which is the difference between the measured differential scattering cross sections of the leucine solution and the water blank shown in *A*. The residual structure in the excess scattering curve centered at $Q \approx 1.9$ Å^{-1} indicates that water structure for the solution is measurably different from that for pure water.

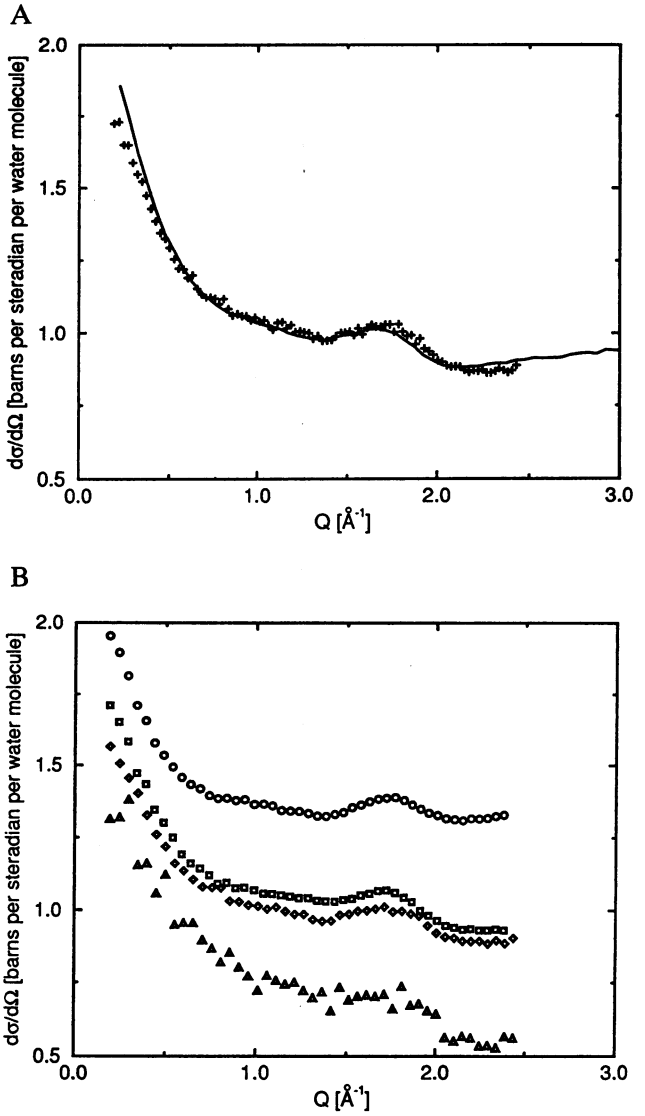

FIG. 2. (*A*) Excess scattering intensity for 0.5 M NALA: data collected at ISIS (solid line) and at HFBR (+). The close agreement indicates that the measurements are not sensitive to differences in the experimental setup. The HFBR data have been scaled to the ISIS data of Fig. 1*B*. (*B*) Excess scattering intensity for aqueous solutions of NALA collected at HFBR. Shown are data from four runs at concentrations of 0.125 M (△), 0.5 M (◇ and □), and 1.0 M (○). The 1.0 and 0.125 M curves have been divided by two and multiplied by four, respectively, and then displaced from the 0.5 M curves for clarity. When scaled in this way, the data show that the perturbation of the water ring is insensitive to solute concentration. The experimental data shown in *A* are represented by the diamonds in *B*.

ring is due to the difference, $\Delta I_{\text{water-water}}(Q)$, in the scattering by water for the aqueous solution (see Eq. **4**) and for pure water.

Fig. 2*A* shows the excess scattering from a 0.5 M NALA solution measured at HFBR. Since the H3B beamline uses an area detector, while SANDALS is a time-of-flight spectrometer, the measured range of momentum transfer is much greater for the latter. As a result the range in Q shown in Fig. 2 is equivalent to the first one-tenth of the range shown in Fig. 1*B*. When the excess scattering curve measured at HFBR is scaled to that measured at ISIS over the range of Q that they cover in common, there is excellent agreement, indicating little sensitivity of the results to the experimental setup.

The perturbation of the scattering intensity across the water ring appears to be relatively insensitive to the NALA concentration over the range from 0.125 to 1.0 M. The consistent shape and amplitude of the ripple, whose inflection point is centered at $Q \approx 1.9$ Å^{-1}, is shown in Fig. 2*B* for four independent experiments conducted at the HFBR. These results, in combination with the data in Fig. 1 for 0.5 M NALA obtained with the SANDALS spectrometer, demonstrate the experimental reproducibility of this phenomenon.

In the absence of any spatial correlations between the solute molecules in the sample or between the solute molecules and water, the excess scattering would be proportional to the spherically averaged molecular structure factor, $\langle F^2_{\text{solute}}(Q)\rangle$. To calculate the molecular structure factors, the x-ray crystal structure of NALA (28) was first used to calculate the spherically averaged square of the Fourier transform of the spatial positions and values of neutron scattering lengths within the molecule. A library of conformations (29) was then used to

calculate the molecular structure factor using a total of 589 conformations from 10,491 occurrences of a leucine sidechain in the data base. A comparison between the molecular structure factor and the experimental data is shown in Fig. 3. The experimentally observed structure in the scattering curve that is seen in the region of the water ring is not present in the molecular structure factor for NALA, which is nearly flat at these angles. This comparison shows that the perturbation in scattering in the region of the water ring is truly due to a change in structure within the hydration shell rather than a trivial effect due to the solute molecule alone.

Additional experiments have been performed with different solutes to determine which part of the molecule (side chain or backbone) is responsible for the observed changes in water structure. Isobutanol and NAGA were chosen because they are roughly equivalent to the side chain and backbone portions of NALA, respectively. Similar measurements were also made for two hydrophilic solutes, NAKA and NAQA; while NAKA is charged at neutral pH, NAQA is not. The excess scattering intensities measured for these solutes are shown in Fig. 4. The bump and dip seen originally in the excess scattering curve for NALA are also quite evident in the curve for isobutanol, but not in the curve for NAGA. This observation establishes that the change in the structure of water occurs around the side chain of NALA, rather than around its "peptide backbone." The bump and dip observed in the region of the water ring are also just detectable in the curve for NAKA, although with a much smaller amplitude and possibly a shifted position, while there is no measurable effect seen in the excess scattering for NAQA. The presence of a reduced perturbation in the water ring for NAKA could possibly be due to the hydrophobic butyl (i.e., C_4H_8) "linker" that connects the ε-amino group to the α-carbon. NAQA, on the other hand, has only a shorter, ethyl (i.e., C_2H_4) linker between the polar amide group and the α-carbon, and a perturbation of the water ring is no longer experimentally detected in this case.

If the perturbed scattering feature in the water ring is strictly due to differently organized solvation shells, such a change should be present for molecular dynamics simulations using a *single* solute molecule in water. Fig. 5 presents the contributions to the excess scattering that can be attributed separately to (*i*) structural changes in water, and (*ii*) solute-water correlations, as derived from simulations for *N*-acetylleucine methylamide and *N*-acetylglutamine methylamide, respectively. Evidently, the structural changes of hydration water that occur in the simulation in turn produce calculated changes in neutron scattering in the water ring that are like those observed experimentally. Distinct positive and negative peaks are seen for the hydrophobic leucine side chain, whereas the effect for the hydrophilic glutamine side chain is much smaller. While the solute-water correlations in the simulation produce a dip in the small angle scattering, their contribution is very flat in the region of the water ring. The good quantitative agreement between the molecular dynamics simulation of a single solute molecule and the experimentally measured perturbation provides clear confirmation that the shift in the peak of the water ring is due to structural changes in water caused by the hydrophobic amino acid side chains, and not due to trivial effects of solute-water scattering.

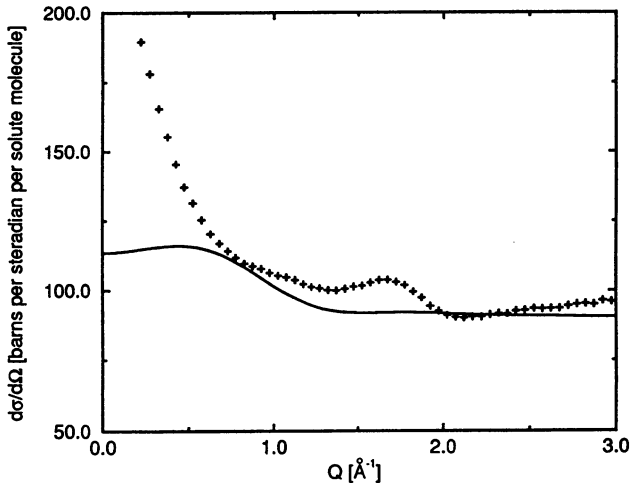

FIG. 3. Excess scattering intensity for 0.50 M NALA expressed as the differential scattering cross section per solute molecule and with the molecular structure factor shown as a solid line for comparison. Since the measured scattering contains isotropic contributions from individual atoms and from incoherent scattering effects, the molecular structure factor was calculated to take both into account. This comparison establishes that the perturbation observed in the water ring is not due to a trivial effect in which the intramolecular scattering from individual solute molecules coincidentally shows interference effects at the same scattering angle as that of the water ring.

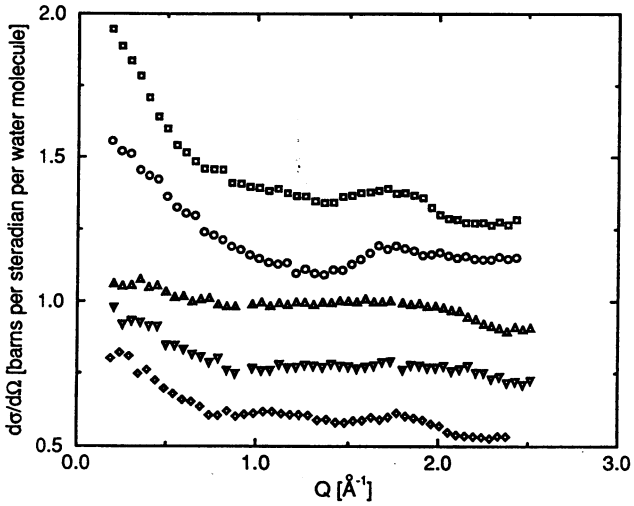

FIG. 4. Comparison of $I_{excess}(Q)$ curves for different amino acid derivatives, without compensation for changes in the structure of water, if any. 0.50 M NALA (□), 0.50 M isobutanol (○), 0.43 M NAGA (△), 0.26 M NAQA (▽), and 0.5 M NAKA (◇). The curves have been scaled (when necessary) to a concentration of 0.5 M and then separated along the x axis for comparison. As explained in the text, these additional measurements narrow down the solute-induced perturbation of the water ring to the hydrophobic character of isobutanol, leucine, and (apparently) the *n*-butyl "linker" of the lysine side chain. All data were collected with the area detector on beamline H3B at the HFBR.

CONCLUSIONS

Both the experimental scattering data and the results of molecular dynamics simulations show that the structure of water within the hydration shell of hydrophobic, but not hydrophilic, amino acid side chains is expanded in comparison to the structure of pure water. It is important to note that we are not necessarily implying a volume expansion, i.e., a decrease in mass density, but instead are referring to a structural deviation from bent and strained hydrogen bonds to hydrogen bonds that are more linear and unstrained. This solute-induced expansion of solvent structure associated with a nonpolar group is complementary to the compression (electrostriction) of water structure, equivalent to that produced by a static pressure of more than a thousand atmospheres, that has been observed at high salt concentration (23). Because NAQA or NAGA are neither strongly hydrophobic nor ionic, it does not seem surprising that the perturbation of the water ring should be small or absent in these cases. For NAKA, the interaction

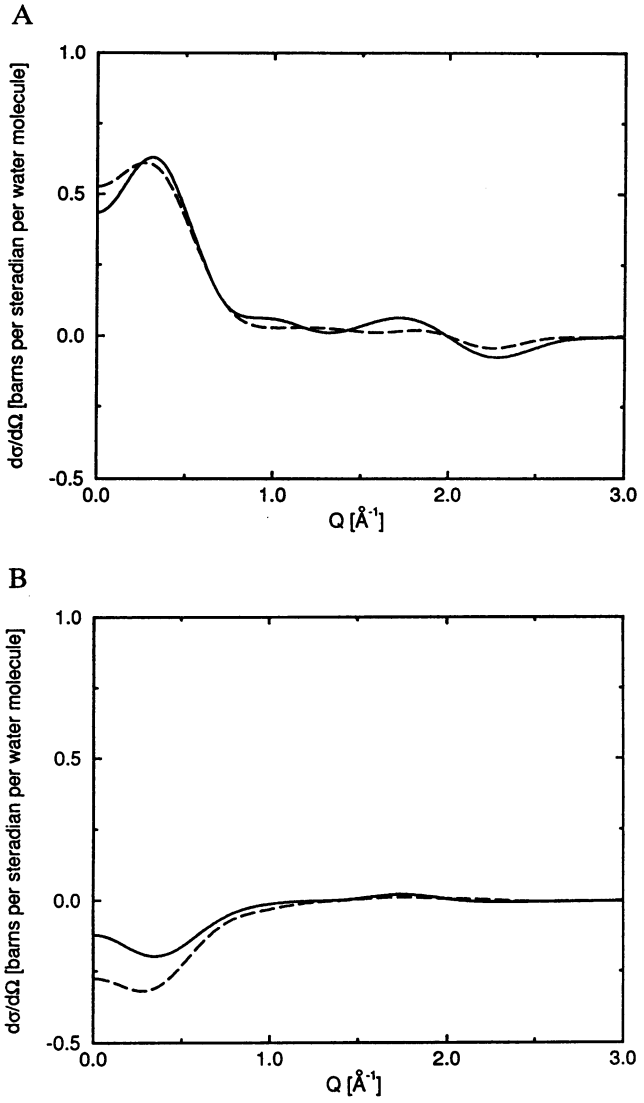

FIG. 5. Simulation results for *N*-acetylleucine methylamide (solid line) and *N*-acetylglutamine methylamide (dashed line). (*A*) Excess scattering due solely to water–water correlations. The rise in scattering at low Q reflects the effects of excluded volume in the solvent and does not include solute–solute and solute–solvent terms. It therefore should not be compared with the small angle scattering shown in the experimental results. The important feature shown in this panel is the nearly quantitative agreement in the excess scattering within the water ring (1.0 Å^{-1} ≤ Q ≤ 3.0 Å^{-1}) when the experimental data are compared with the simulated contribution arising from just the water. (*B*) Excess scattering due solely to solute–water correlations. The important feature shown is the fact that the solute–water correlations make no significant contribution in the region of the water ring. The high Q limit is zero in both cases because the isotropic scattering from individual atoms and from incoherent scattering effects has not been added to the calculated curves.

of water with the hydrophobic C_4H_8 butyl linker of the side chain apparently dominates the solvation of the $NH_3^+Cl^-$ ion pair, resulting in a net shift of the water ring to smaller angle.

The shift of the peak of the water ring to lower Q reported here is qualitatively similar to the same directional shift of the main neutron diffraction peak measured for supercooled water with respect to the ambient temperature liquid (18–20). The neutron scattering experiments on pure water (18–20) and our results provide evidence for a similar geometric water structure between supercooled water and hydration water near hydrophobic groups. Further analysis of the molecular dynamics results is needed to show that the structural organization of water near hydrophobic species is due to the formation of unstrained hydrogen-bonded polyhedra (2) and/or self-replicating pentagons (21, 22).

The good agreement between the measured scattering curves and those calculated from molecular dynamics simulations gives important cross-validation between the two results. Further analysis of these simulations, including the polygon analysis developed recently to understand hydration structure around hydrophobic groups (17), could provide a molecular interpretation of the experimental scattering data. Furthermore, the agreement between simulations and scattering data establishes that it will be worthwhile to use the simulations to quantify structural changes that occur in successive layers of the hydration shell, thus characterizing the range, or persistence length, of the structural changes that have long been believed to occur at the surface of hydrophobic side chains.

The idea that the water in the hydration sphere of hydrophobic groups has a different structure from that of bulk water supports a model that attributes long-range hydration forces to the elimination of ordered solvent when two solute molecules begin to approach one another, and the mean attraction between hydrogen-bonded polyhedral cages which drives them to cluster together (2). The further demonstration that alterations in water structure around hydrophobic amino acid side chains are long-ranged and thermodynamically significant would have a profound impact on our understanding of the early stages of protein folding (30, 31).

We acknowledge support from the Committee on Research of the University of California at Berkeley and from National Institutes of Health training grants in molecular biophysics and biotechnology. We thank the National Energy Research Supercomputer Center for computer time. Part of this work was conducted at the High Flux Beam Reactor, Brookhaven National Laboratory, and was supported by the Division of Materials Sciences, U.S. Department of Energy, under Contract No. DE-AC02-76CH00016.

1. Franks, F. (1975) in *Water: A Comprehensive Treatise*, ed. Franks, F. (Plenum, New York). Vols. 2 and 4.
2. Stillinger, F. H. (1980) *Science* **209,** 451–455.
3. Murphy, K. P., Privalov, P. L. & Gill, S. J. (1990) *Science* **247,** 559–561.
4. Livingstone, J. R., Spolar, R. S. & Record, M. T., Jr. (1991) *Biochemistry* **30,** 4237–4244.
5. Keener, C. R., Fullerton, G. D., Cameron, I. L. & Xiong, J. (1995) *Biophys. J.* **68,** 291–302.
6. Pratt, L. R. & Chandler, D. (1977) *J. Chem. Phys.* **67,** 3683–3704.
7. Stillinger, F. H. (1973) *J. Soln. Chem.* **2,** 141–158.
8. Owicki, J. C. & Scheraga, H. A. (1977) *J. Am. Chem. Soc.* **99,** 7413–7418.
9. Swaminathan, S., Harrison, S. W. & Beveridge, D. L. (1978) *J. Am. Chem. Soc.* **100,** 5705–5712.
10. Geiger, A., Rahman, A. & Stillinger, F. H. (1979) *J. Chem. Phys.* **70,** 263–276.
11. Pangali, C., Rao, M. & Berne, B. J. (1979) *J. Chem. Phys.* **71,** 2975–2981.
12. Zichi, D. A. & Rossky. P. J. (1985) *J. Chem. Phys.* **83,** 797–808.
13. Guillot, B. & Guissani, Y. (1993) *J. Chem. Phys.* **99,** 8075–8094.
14. Turner, J. & Soper, A. K. (1994) *J. Chem. Phys.* **101,** 6116–6125.
15. Turner, J., Soper, A. K. & Finney, J. L. (1995) *J. Chem. Phys.* **102,** 5438–5443.
16. Davidson, D. W. (1973) in *Water: A Comprehensive Treatise*, ed. Franks, F. (Plenum, New York), Vol. 2, pp. 115–145.
17. Head-Gordon, T. (1995) *Proc. Natl. Acad. Sci. USA* **92,** 8308–8312.
18. Dore, J. C. (1990) *J. Mol. Struct.* **237,** 221–232.
19. Bosio, L., Teixeira, J., Dore, J. C., Steytler, D. & Chieux, P. (1983) *Mol. Phys.* **50,** 733–740.
20. Bellissent-Funel, M.-C., Teixeira, J., Bosio, L., Dore, J. & Chieux, P. (1986) *Europhys. Lett.* **2,** 241–245.
21. Speedy, R. J. (1984) *J. Phys. Chem.* **88,** 3364–3373.
22. Mettananda, I. H. I. U. & Speedy, R. J. (1984) *J. Phys. Chem.* **88,** 4163–4166.
23. Leberman, R. & Soper, A. K. (1995) *Nature (London)* **378,** 364–366.

24. Pertsemlidis, A. (1995) Ph.D. thesis, (Univ. of California, Berkeley).
25. Soper, A. K., Howells, W. S. & Hannon, A. C. (1989) ATLAS, Analysis of Time-of-Flight Neutron Diffraction Data From Liquid and Amorphous Samples (Rutherford Appleton Laboratory, Didcot, U.K.), Report no. 89–046.
26. Cornell, W. D., Cieplak, P., Bayly, C. I., Gould, I. R., Merz, K. M., Ferguson, D. M., Spellmeyer, D. C., Fox, T., Caldwell, J. W. & Kollman, P. A. (1995) *J. Am. Chem. Soc.* **117,** 5179–5197.
27. Berendsen, H. J. C., Postma, J. P. M., van Gunsteren, W. F. & Hermanns, J. (1981) in *Intermolecular Forces*, ed. Pullman, B. (Reidel, Dordrecht, The Netherlannds), p. 331.
28. Puliti, R., Mattia, C. A., Barone, G. & Giancola, C. (1991) *Acta Crystallogr.* **C47,** 1658–1662.
29. Dunbrack, R. L., Jr., & Karplus, M. (1994) *Nature (London) Struct. Biol.* **1,** 334–340.
30. Kauzmann, W. (1959) *Adv. Protein Chem.* **14,** 1–63.
31. Dill, K. A. (1990) *Biochemistry* **29,** 7133–7155.